Acta Pharmaceutica Sinica B 2024;14(5):2026–2038

Chinese Pharmaceutical Association
Institute of Materia Medica, Chinese Academy of Medical Sciences

Acta Pharmaceutica Sinica B

www.elsevier.com/locate/apsb
www.sciencedirect.com

ORIGINAL ARTICLE

ALS-linked C9orf72 dipeptide repeats inhibit starvation-induced autophagy through modulating BCL2–BECN1 interaction

Shiqiang Xu[a,†], Qilian Ma[a,d,†], Junwen Shen[a], Ningning Li[a], Shan Sun[a,e], Nana Wang[a], Yang Chen[a], Chunsheng Dong[f], Kin Yip Tam[e], Jochen H.M. Prehn[d], Hongfeng Wang[a,b,*], Zheng Ying[a,b,c,*]

[a]*Jiangsu Key Laboratory of Neuropsychiatric Diseases and College of Pharmaceutical Sciences, Soochow University, Suzhou 215123, China*
[b]*MOE Key Laboratory of Geriatric Diseases and Immunology, College of Pharmaceutical Sciences, Suzhou Medical College of Soochow University, Suzhou 215123, China*
[c]*Jiangsu Province Engineering Research Center of Precision Diagnostics and Therapeutics Development, Soochow University, Suzhou 215123, China*
[d]*Dept. of Physiology & Medical Physics and FUTURE-NEURO Research Centre, Royal College of Surgeons in Ireland, Dublin D02 YN77, Ireland*
[e]*Faculty of Health Sciences, University of Macau, Taipa, Macau 999078, China*
[f]*Insititutes of Biology and Medical Science, Soochow University, Suzhou 215123, China*

Received 9 October 2023; received in revised form 24 January 2024; accepted 30 January 2024

KEY WORDS

Amyotrophic lateral sclerosis;
Frontotemporal dementia;
C9orf72;
Autophagy;

Abstract Growing evidences indicate that dysfunction of autophagy contributes to the disease pathogenesis of amyotrophic lateral sclerosis (ALS) and frontotemporal dementia (FTD), two neurodegenerative disorders. The GGGGCC·GGCCCC repeat RNA expansion in chromosome 9 open reading frame 72 (*C9orf72*) is the most genetic cause of both ALS and FTD. According to the previous studies, GGGGCC·GGCCCC repeat undergoes the unconventional repeat-associated non-ATG translation, which produces dipeptide repeat (DPR) proteins. Although there is a growing understanding that *C9orf72* DPRs

*Corresponding authors.
E-mail addresses: zheng.ying@suda.edu.cn (Zheng Ying), wanghongfeng@suda.edu.cn (Hongfeng Wang).
[†]These authors made equal contributions to this work.
Peer review under the responsibility of Chinese Pharmaceutical Association and Institute of Materia Medica, Chinese Academy of Medical Sciences.

https://doi.org/10.1016/j.apsb.2024.02.004

BCL2;
BECN1/Beclin 1;
Dipeptide repeat;
Neurodegeneration

have a strong ability to harm neurons and induce *C9orf72*-linked ALS/FTD, whether these DPRs can affect autophagy remains unclear. In the present study, we find that poly-GR and poly-PR, two arginine-containing DPRs which display the most cytotoxic properties according to the previous studies, strongly inhibit starvation-induced autophagy. Moreover, our data indicate that arginine-rich DPRs enhance the interaction between BCL2 and BECN1/Beclin 1 by inhibiting BCL2 phosphorylation, therefore they can impair autophagic clearance of neurodegenerative disease-associated protein aggregates under starvation condition in cells. Importantly, our study not only highlights the role of *C9orf72* DPR in autophagy dysfunction, but also provides novel insight that pharmacological intervention of autophagy using SW063058, a small molecule compound that can disrupt the interaction between BECN1 and BCL2, may reduce *C9orf72* DPR-induced neurotoxicity.

1. Introduction

Amyotrophic lateral sclerosis (ALS), also known as Lou Gehrig's disease, is a devastating neurodegenerative disease which shares genetic and pathological overlaps with frontotemporal lobar degeneration (FTD). ALS results from the degeneration of lower and upper motor neurons, and is characterized by rapidly progressive paralysis and death from respiratory failure[1,2]. At present, there is no effective medicine and clinical treatment that can cure ALS. According to the previous study, approximately 90% of ALS patients are classified as sporadic, whereas the remaining 10% of patients are identified as familial[1,2]. GGGGCC hexanucleotide repeat expansions in noncoding region of chromosome 9 open reading frame 72 (*C9orf72* gene) has been considered as the most common cause of familial ALS[3–5]. Surprisingly, from repeat-associated non-ATG (RAN) translation, the bidirectional GGGGCC and GGCCCC hexanucleotide repeat expansions encode five dipeptide repeats (DPRs), poly-glycine-alanine (GA), glycine-proline (GP), glycine-arginine (GR), proline-arginine (PR) and proline-alanine (PA). Those RAN-translated DPRs are expressed in the affected tissue of ALS/FTD patients, which indicates that DPRs may play important roles in disease pathogenesis[2,6]. According to recent studies, two arginine-rich DPRs, poly-GR and poly-PR, are the most toxic proteins among all the DPRs translated from *C9orf72* hexanucleotide repeats[6–11].

Autophagy−lysosome pathway (ALP) is an evolutionally conserved process that is essential for cellular metabolic homeostasis and quality control, and autophagy dysfunction is observed in various neurodegenerative diseases including ALS[12,13]. Previous studies showed that knockout of autophagy-related genes, such as ATG5 or ATG7, in the central nervous system, can lead to progressive motor deficits in mouse models[14,15]. Those mice exhibited ubiquitin-positive protein aggregates formed by misfolded proteins, which are key features of neurodegenerative diseases, including Huntington's disease and ALS. Importantly, increasing evidence indicates that autophagy is abnormally regulated by ALS/FTD-associated proteins, and mutations in autophagy receptors, such as p62/SQSTM1 and OPTN, genetically cause ALS[16]. However, whether and how *C9orf72* DPRs affect autophagy remains largely unknown.

To further understand the relationship between autophagy and the *C9orf72* DPRs, we studied the effects of five DPRs on autophagy in cellular and mouse model. In our current study, we find that the two arginine-rich DPRs, poly-GR and poly-PR, impair the initiation step of the autophagosome formation by regulating BCL2−BECN1 interaction in association with BCL2 phosphorylation. The BH3 mimetic compound SW063058 effectively inhibits the BECN1−BCL2 interaction and alleviates autophagy impairment driven by poly-GR and poly-PR. Intriguingly, poly-GR and poly-PR also reduce the mTORC1 (mechanistic target of rapamycin kinase complex 1) activity and enhance TFEB nuclear translocation, as shown in models of protein loss of function associated with ALS[17–20]. In addition, we found that *C9orf72* arginine-rich DPR blocks autophagic turnover and increases pathogenic protein aggregation in starved cells. Taken together, our study shows that *C9orf72*-linked poly-GR and poly-PR can impair autophagy through enhancing BECN1−BCL2 binding and impede the quality control of protein aggregates, suggesting that autophagy dysfunction may contribute to *C9orf72* DPR-mediated pathogenesis, similarly as other ALS/FTD cases.

2. Materials and methods

2.1. Plasmid constructions

GFP, GFP-TFEB, GFP-BCL2, GFP-LC3, GFP-Htt-60Q, GFP-Htt-150Q, GFP-BCL2, FLAG, FLAG-BECN1, mCherry, mCherry-GFP-LC3B, GFP-GAggagca (GA*30), GFP-GRggaaga (GR*30), GFP-PRccaaga (PR*30), Flag-GAggagca (GA*30), Flag-GRggaaga (GR*30) and mCherry-PRccccgg (PR*46) plasmids were described previously[11,17,20–24]. mCherry-LC3B was a gift from Dr. David Rubinsztein (Addgene plasmid #40827). pMRX-IP-GFP-LC3-RFP-LC3ΔG was a gift from Dr. Mizushima (Addgene plasmid #84572). ATG5-GFP, ATG9-GFP, DFCP1-GFP and ATG16-mCherry were kindly provided by Dr. Quanhong Ma (Soochow University, China). GABARAPL1 cDNA was first amplified using PCR from a human fetal brain cDNA library (Clontech) using the primers 5′-GAAGATCTACCATGAAG TTCGTGTAC-3′ and 5′-GCGTCGACTCACAGACCGTAGAC-3′. The PCR product was subsequently inserted into the p3xFLAG-Myc-CMV-24 (Sigma) vector at the Bgl II/Sal I sites.

2.2. Cell culture, transfection and drug treatment

Human embryonic kidney 293 cells (HEK293), Human embryonic kidney 293T cells (HEK293T), Human cervical cancer cells (HeLa), ATG5 WT, and KO mouse embryonic fibroblast (MEF) cells were cultured in Dulbecco's modified Eagle's medium (DMEM) (Gibco) containing 10% fetal bovine serum (FBS) (Gibco) with streptomycin (100 μg/mL) and Penicillin

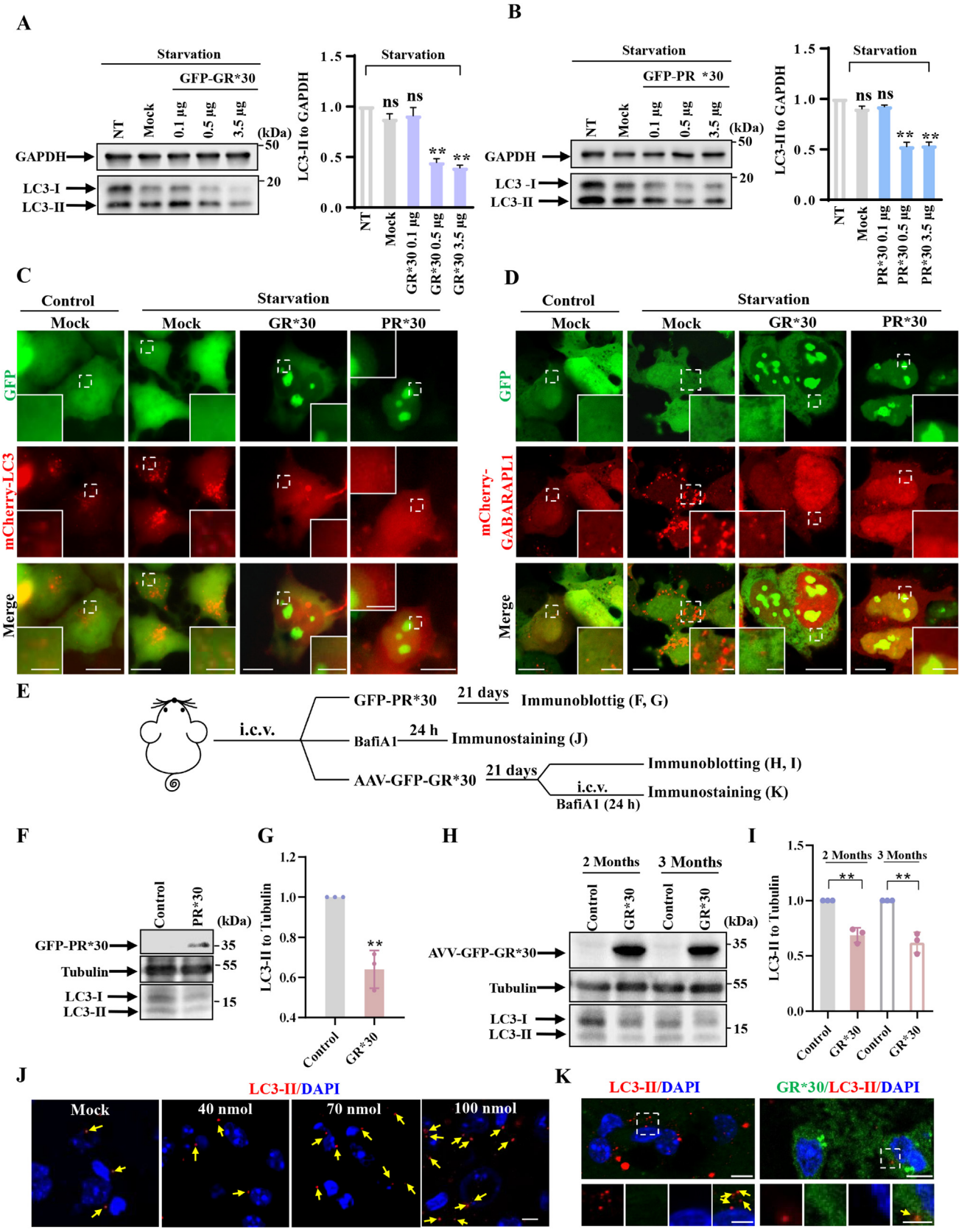

Figure 1 *C9orf72*-linked poly-GR and poly-PR inhibit the formation of autophagosomes under starvation condition. (A, B) HEK 293 cells were transfected with 0.1, 0.5 or 3.5 μg GFP-GR*30, GFP-PR*30 or GFP tag. After 48 h, the cells were incubated with Earle's balanced salt solution (EBSS) for 1 h, and cell lysates were subjected to immunoblot analysis using antibodies against GAPDH and LC3. Quantification of the relative intensity of LC3-II to GAPDH. Data from three independent experiments are represented as means ± SEM, ns, not significantly different;

(100 U/mL). Primary mouse cortical neurons were harvest as described[25]. Lipofectamine RNAiMAX transfection reagent (Invitrogen) was applied for siRNAs transfection upon cell splitting, the cells were transfected with Lipofectamine 2000 transfection reagent (Invitrogen) in Opti-MEM (Invitrogen) without serum according to the manufacturer's instructions. Cells were starved with Earle's balanced salt solution (EBSS) (Gibco) for 1 h. Cells were treated with DMSO (BBI Life Science Corporation), 250 nmol/L Torin-1 (Tocris Bioscience) for 1 h, 100 nmol/L Bafilomycin A1 (Sigma) for 12 h, or SW063058 (Sigma) for 12 h.

2.3. Intracerebroventricular injections in C57BL/6 mice

AAV-PHP.eB-CAG>Kozak-EGFP-GGAAGA Repeat (GR*30) was generated by Cyagen Bioscience. Two microliters of AAV were injected into right lateral cerebral ventricle of 2-month or 3-month mouse brain through intracerebroventricular injection at the flow rate of 0.2 μL/min. Bafilomycin A1 (40 nmol, 70 nmol and 100 nmol in 2 μL PBS) were injected into mouse brain at the flow rate of 0.2 μL/min. Stereotaxic injection of 1.5 μg endotoxin free DNA of EGFP-PR*30 mixing with *in vivo*-jetPEI (Polyplus) at $N/P = 7$ into right lateral cerebral ventricle of 4-months mouse brain (0.2 μL/min).

2.4. Antibodies

The following primary antibodies were used: anti-FLAG antibody (Sigma), anti-GFP antibody (Santa Cruz), anti-GAPDH antibody (Millipore), anti-phospho-p70S6K (T389) antibody (Cell Signaling Technology), anti-p70S6K antibody (Epitomics), anti-mTOR antibody (Cell Signaling Technology), anti-LC3B antibody (Novus Biologicals), anti-LC3B antibody (Abcam), anti-GAPDH antibody (Proteintech), anti-Tubulin antibody (Proteintech), anti-MAP2 antibody (Proteintech), anti-LAMP2 antibody (Santa Cruz), anti-Bcl2 (total, pS70 or pS87) antibody (Santa Cruz) and anti-BECN1 antibody (Santa Cruz). The following secondary antibodies were used: horseradish peroxidase-conjugated sheep anti-mouse and anti-rabbit antibodies (Jackson ImmunoResearch Laboratories) for immunoblotting and Alexa Fluor 594-conjugated AffiniPure Donkey Anti-Mouse IgG antibody (Proteintech), Alexa Fluor 594-conjugated AffiniPure Donkey Anti-Rabbit IgG antibody (Proteintech) or Alexa Fluor 647-conjugated AffiniPure Donkey Anti-Rabbit IgG antibody (Yasen Biotechnology) for immunocytochemistry and immunohistochemistry. DAPI (Sigma) or Hoechst (Sigma) were used for nuclei staining.

2.5. Immunoblot

The cells were collected at indicated time after transfection and were lysed in the cell lysis buffer containing 50 mmol/L Tris-HCl (pH 7.6) with protease inhibitor cocktail (Roche), 150 mmol/L NaCl, 0.5% sodium deoxycholate, and 1% Nonidet P-40. Proteins were separated by 10%, 12%, 13.5% or 15% SDS−PAGE (polyacrylamide gel electrophoresis) and transferred onto a PVDF membrane (polyvinylidene difluoride membrane; Millipore). Samples were sequentially incubated by primary antibodies and secondary antibodies. Proteins were visualized by ECL kit (Thermo Fisher Scientific).

2.6. Immunocytochemistry, immunohistochemistry and live cell imaging

For immunocytochemistry assay, the cells were washed with pre-warmed PBS and fixed with 4% paraformaldehyde in PBS at room temperature for 5−10 min. Cells were permeabilized with 0.1% Triton X-100 in PBS for 5 min and blocked for 20 min with 0.2% FBS in PBST. Then the cells were incubated with primary antibody diluted with PBST at room temperature for 4 h, washed lightly with PBST for 5 min. Then the cells were incubated with secondary antibody for 2 h at room temperature. For immunohistochemistry assay, mouse brains were fixed with 4% paraformaldehyde in PBS at 4 °C for 24 h, followed by dehydration with 30% sucrose in PBS at 4 °C for 24 h. Then, the brains were embedded with O.T.C. compound (SAKURA), frozen on liquid nitrogen and stored at −80 °C for cryosections (18 μm). Sections were permeabilized with 0.4% Triton X-100 in PBS for 1 h and blocked for 2 min with 4% FBS and 0.4% Triton X-100 in PBST. Tissues were incubated with anti-LC3B antibody (Abcam) at 4 °C overnight and secondary antibody for 4 h at room temperature. DAPI (blue) was added for incubation for 3 min at room temperature to visualize the nuclei. Finally, the immune-stained cells, tissues or live cells were imaged using fluorescent microscope (Nikon ECLIPSE TE2000-E or Ti2-E) or a Zeiss confocal microscope[26,27].

2.7. Immunoprecipitation

HEK293T cells transfected with the indicated plasmids were collected 24 h after transfection and lysed in cell lysis buffer. Cell pellets were discarded after centrifugation at 12,000×*g* for 15 min at 4 °C, and the supernatants were used for immunoprecipitation.

**$P < 0.01$, one-way ANOVA. NT indicates no transfection. (C, D) HEK 293 cells were transfected with GFP, GFP-GR*30 or GFP-PR*30, along with mCherry-LC3 or mCherry-GABARAPL1. After 24 h, the cells were incubated with EBSS or normal culture medium for 1 h and visualized using fluorescence microscopy. Scale bar, 10 μm. Insets were higher magnifications of the dashed box area. Scale bars, 2 μm. (E) Experimental design of assessing autophagy level in mouse model. (F) C57BL/6 mice at 4 months were injected *in vivo*-jetPEI mixed with or without GFP-PR*30 in right lateral cerebral ventricle. Mice were sacrificed after 21 days and the brain lysates were subjected to immunoblot analysis using antibodies against GFP, Tubulin and LC3 ($n = 3$ animals per group). (G) Quantification of the relative intensity of LC3-II to Tubulin in F. Data from three independent experiments are represented as means ± SD; **$P < 0.01$, one-way ANOVA. (H) C57BL/6 mice at 2 months or 3 months were injected with or without AAV-GFP-GR*30 in right lateral cerebral ventricle. Mice were sacrificed after 21 days and the brain lysates were subjected to immunoblot analysis using antibodies against GFP, Tubulin and LC3 ($n = 3$ animals per group). (I) Quantification of the relative intensity of LC3-II to Tubulin in (H). Data from three independent experiments are represented as means ± SD; **$P < 0.01$, one-way ANOVA. (J) C57BL/6 mice at 2 months were injected with BafiA1 (40 or 70 or 100 nmol). Mice were sacrificed after 24 h and subjected to immunostaining analysis using antibodies against LC3 ($n = 3$ animals per group), yellow arrows indicate LC3-positive autophagosomes. (K) C57BL/6 mice at 2 months were injected with or without AAV-GFP-GR*30 in right lateral cerebral ventricle and injected with 100 nmol BafiA1 after 20 days. Mice were sacrificed after 24 h and subjected to immunostaining analysis using antibodies against LC3 ($n = 3$ animals per group), yellow arrows indicate LC3-positive autophagosomes. Scale bar, 10 μm. Insets were higher magnifications of the dashed box area. Scale bars, 5 μm.

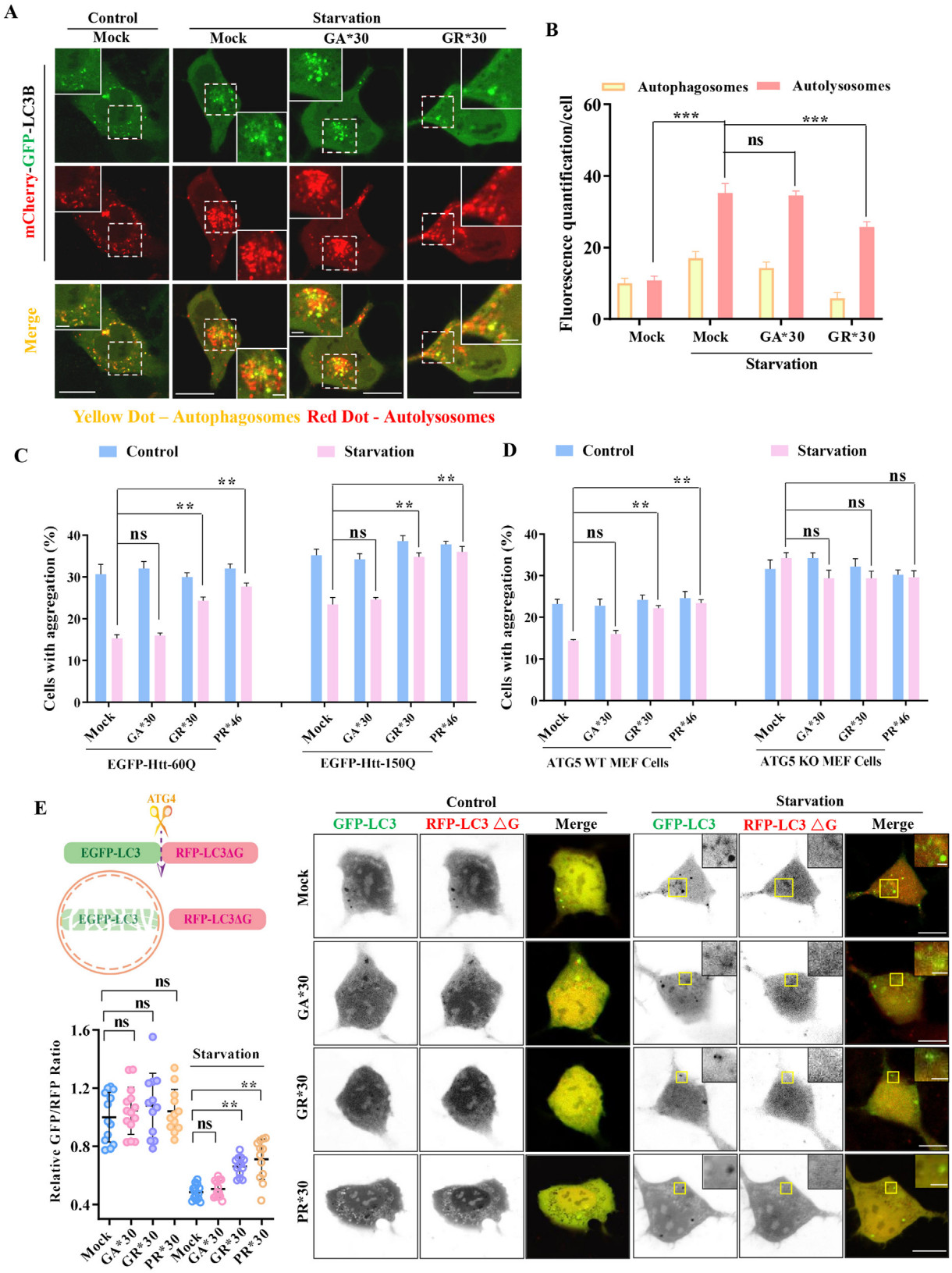

Figure 2 Poly-GR and poly-PR inhibit the autophagic clearance of poly-Q proteins. (A, B) HEK 293 cells were transfected with mCherry-GFP-LC3 and FLAG-GA*30, FLAG-GR*30 or FLAG tag. After 24 h, the cells were incubated with normal culture medium or EBSS for 1 h. Cells were visualized using confocal microscopy. Scale bars, 10 μm. Insets were higher magnifications of the dashed box area. Scale bars, 2 μm. The quantitative data of yellow dots (autophagosomes) or red dots (autolysosomes) are shown in (B). Data from three independent experiments represented as means ± SEM; ***$P < 0.001$, one-way ANOVA. (C) HEK 293 cells were transfected with GFP-Htt-60Q or GFP-Htt-150Q, along with FLAG-GA*30, FLAG-GR*30, mCherry-PR*46 or FLAG tag (Mock). After 12 h, the cells were incubated with normal culture

The protein G Sepharose (Roche) or Protein A/G Magnetic Beads (Biotool) were incubated with anti-GFP or anti-FLAG antibody at 4 °C for 4 h, and then washed twice with PBS and incubated with cell supernatants for 4 h at 4 °C. The beads were washed three times with cell lysis buffer. Then, the proteins were eluted with SDS sample buffer for immunoblot analysis.

2.8. *In situ proximity ligation assay (PLA)*

4% paraformaldehyde and 0.1% Triton X-100 were applied for cells fixation and permeabilization. The cells were incubated with the BECN1 antibody (BBI Life Science Corporation) and BCL2 antibody (Santa Cruz). Duolink in situ PLA kit were used for the next step according to the manufacturer's instructions (Duolink® In Situ Red, Sigma−Aldrich). The cells were visualized by a Nikon fluorescent microscope (Ti2-E) and images were captured using a sCMOS camera (pco.edge 4.2 bi).

2.9. *Statistical analysis*

The Photoshop 7.0 (Adobe) software was used to perform immunoblot densitometric analyses of three independent experiments. The obtained data were used for generating charts using Prism 9.0 (GraphPad Software) software. *P*-values were indicated in figure legends.

3. Results

3.1. *C9orf72-linked poly-GR and poly-PR, two arginine-containing DPRs, reduce the numbers of autophagic vesicles under starvation condition*

Autophagy plays an important role in neurodegenerative disease including ALS/FTD. To understand the relationship between *C9orf72*-linked ALS/FTD and autophagy, we first tested whether the five DPRs could influence autophagy. In cells overexpressing different doses of *C9orf72* arginine-containing poly-GR and poly-PR, the protein level of microtubule associated protein 1 light chain 3 beta-II (MAP1LC3B/LC3B-II, hereafter referred to as LC3-II), which is the marker of cellular autophagic vesicles, was strikingly decreased under starvation condition (Fig. 1A and B). Whereas, LC3-II level was not reduced in other *C9orf72* DPR (poly-GA, poly-PA or poly-GP)-expressing cells (data not shown). These data suggest that expression of poly-GR and poly-PR may reduce the numbers of autophagic vesicles. To further confirm this hypothesis, we tested the influence of different amount of poly-GR and poly-PR on the formation of autophagosomes. The data indicate that poly-GR and poly-PR can decrease the protein level of LC3-II in a dose-dependent manner under starvation condition (Fig. 1A and B). Furthermore, immunofluorescence showed that poly-GR and poly-PR could strikingly decrease the numbers of LC3B and GABARAPL1 (GABA type A receptor-associated protein like 1)-positive autophagosomes in starved cells (Fig. 1C and D, Supporting Information Fig. S1). To further assess the effect of DPRs on autophagy *in vivo*, we measured autophagy by detecting LC3 levels in mouse brain expressing poly-GR and poly-PR (Fig. 1E). Our data suggest that LC3-II level was decreased upon poly-PR and poly-GR expression *in vivo* (Fig. 1F−I). Bafilomycin A1 (BafiA1) was employed to amplify autophagosomal accumulation (Fig. 1J). We observed that LC3 dots (which reflects autophagosome numbers) were reduced in the mouse brain expressing poly-GR (Fig. 1K). These results indicated that two arginine-containing DPRs, poly-GR and poly-PR, may impair ALP.

3.2. *Arginine-containing DPRs impair the autophagic flux and the clearance of autophagic substrates*

To further test the effect of poly-GR and poly-PR on autophagic flux, we used mCherry-GFP-LC3 as a reporter of autophagic flux. According to the previous studies, GFP signal quenches in the acidic lysosomes, therefore the yellow dots, which are recognized as the combination of mCherry (red) and GFP (green) signals, indicate autophagosomes, and the red dots indicate autolysosomes[17,28]. Under starvation condition, the numbers of both autophagosomes (yellow dots) and autolysosomes (red dots) were significantly decreased in poly-GR, but not poly-GA-expressing cells, indicating that arginine-containing DPR may inhibit the formation of autophagosomes (Fig. 2A and B). Huntingtin protein containing expanded polyglutamine (poly-Q) can form protein aggregates in cells and can be used as a reporter of autophagic substrate degradation[23]. We therefore tested the aggregation of N-terminus of Huntingtin containing 60 poly-Q (Htt-60Q) and 150 poly-Q (Htt-150Q), which reflects the level of autophagic clearance, in cells expressing *C9orf72* DPRs. Our results indicated that poly-GR and poly-PR inhibited the autophagic clearance of Htt-60Q and Htt-150Q aggregates under starvation condition, whereas poly-GA had no such effect (Fig. 2C, Supporting Information Fig. S2). To confirm the impaired clearance of poly-Q aggregates is related to perturbed autophagy, we did the similar experiment in wild type and *atg5* knockout mouse embryonic fibroblast (MEF) cells. In contrast to the effect in WT MEFs, poly-GR or poly-PR failed to block the clearance of Htt-60Q aggregates in starved *atg5* knockout MEFs, indicating that poly-GR and poly-PR inhibit the autophagic clearance of poly-Q aggregates (Fig. 2D). To test the overall autophagic turnover in poly-GR and poly-PR expressing cells, we employed a fluorescent reporter of autophagic degradation known as GFP-LC3-RFP-LC3ΔG, which is cleaved by ATG4 into GFP-LC3 and RFP-LC3ΔG. GFP-LC3 can be digested in autolysosome, while RFP-LC3 ΔG still stays in cytosol, working as a cellular internal control (Fig. 2E, left upper panel)[29]. The ratio of GFP to RFP reflects autophagy flux[29]. Our experiments demonstrated that

medium or EBSS for 1 h. Then the cells were visualized using fluorescence microscopy. The quantitative data of poly-Q aggregates from three independent experiments are represented as means ± SEM; ns, not significantly different; $^{**}P < 0.01$, one-way ANOVA. (D) Mouse embryonic fibroblast (MEF) cells or ATG5 KO MEF cells were similarly transfected with GFP-Htt-60Q, along with FLAG-GA*30, FLAG-GR*30, mCherry-PR*46 or FLAG tag (Mock). Cells processed as in (C). The quantification data of poly-Q aggregates are shown as means ± SEM; ns, not significantly different; $^{**}P < 0.01$, one-way ANOV. (E) HEK 293 cells were transfected with GFP-LC3-RFP-LC3ΔG and FLAG-GA*30, FLAG-GR*30, FLAG-PR*30 or FLAG tag. After 48 h, the cells were incubated with normal culture medium or EBSS for 1 h. Then, cells were visualized using confocal microscopy. Scale bars, 10 μm. Insets were higher magnifications of the dashed box area. Scale bars, 2 μm. Statistical data from three independent experiments are represented as means ± SEM; ns, not significantly different; $^{**}P < 0.01$, one-way ANOVA.

poly-PR inhibited the turnover of autophagic substrate GFP-LC3, while poly-GA showed little effect on this process (Fig. 2E). Taken together, these data indicate that poly-PR perturbs the overall function of autophagy.

According to the previous studies, active mTORC1 localizes on the lysosomal surface, and mTOR releasing from the lysosomal surface will result in mTOR deactivation and TFEB nuclear translocation, with in turn increase autophagy[18]. To test whether *C9orf72*-linked poly-GR and poly-PR inhibit autophagy by regulating mTOR signaling, we detected the cellular localization of mTOR in cells expressing *C9orf72* DPRs. In control and poly-GA expressing cells, mTOR localized on lysosome (Supporting information Fig. S3A). Surprisingly, mTOR translocated from the lysosome to cytosol when we expressed poly-GR and poly-PR into the cells, indicating that poly-GR and poly-PR inhibited the mTOR lysosomal localization (Fig. S3A). In consistent with these evidences, phosphorylation of p70S6K, a well-recognized mTORC1 substrate, reduced in cells transfected with poly-GR and poly-PR under starvation condition, although autophagy was inhibited (the protein level of LC3-II also decreased) (Fig. S3B−S3D). Note that poly-GR and poly-PR, but not poly-GA, could promote nuclear translocation of TFEB, a well-known autophagy regulator that acts downstream of mTORC1, suggesting that TFEB signaling was activated in these cells (Fig. S3E and S3F). In conclusion, poly-GR and poly-PR inhibit the activity of mTORC1 and promote TFEB nuclear translocation, but doesn't thereby enhance autophagy. These data suggest that the effect of poly-PR and poly-PR on autophagic inhibition is mTORC1 independent.

3.3. *C9orf72 arginine-containing poly-PR inhibits autophagosome formation*

Given that poly-GR and poly-PR may not regulate the formation of autophagosomes *via* mTORC1, to further explore the mechanism, we examined several key factors which function in different steps of autophagy, including ATG9A, ZFYVE1/DFCP1 and ATG5−ATG16[30]. Trafficking of ATG9 from peripheral membrane, Golgi apparatus and endosomes is important for phagophore biogenesis[30]. We firstly examined the localization of ATG9 in cells, and found that starvation decreased the numbers of ATG9 vesicles (indicating ATG9 delivers the membrane materials to the phagophore), whereas poly-PR increased the numbers of ATG9 vesicles in starved cells (Fig. 3A). In addition, poly-PR reduced the vesicle numbers of the phagophore nucleation factor DFCP1 and the phagophore expansion factor ATG5−ATG16 in starved cells (Fig. 3B−G). Taken together, our results suggest that poly-PR inhibits the initiation step of autophagy (autophagosome formation) and target the factors upstream of ATG9, DFCP1 and subsequent phagophore expansion factors.

3.4. *Poly-PR and poly-GR promote the interaction between BECN1 and BCL2 by reducing BCL2 phosphorylation, thereby inhibiting autophagy*

BECN1 is one component of the PI3KC3 complex I which coordinate with ULK1 complex to regulate the initiation and nucleation of phagophore[30]. BCL2 regulates the kinase activity of the BECN1−Vps34 complex by interacting with BECN1 and disrupting the association between BECN1 and Vps34, leading to decreased autophagosome formation[30−32]. To ask whether arginine-rich DPR could affect the interaction between BCL2 and BECN1, we tested the BCL2−BECN1 interaction in poly-PR expressing cells. The immunoblot assay showed that the protein level of BECN1was not changed in cells transfected with poly-PR or poly-GR (Fig. 4A and B). Interestingly, immunoprecipitation assay revealed that the interaction between BCL2 and BECN1 was enhanced by poly-PR expression, indicating that poly-PR inhibited the autophagosome formation by promoting the interaction between BCL2 and BECN1 (Fig. 4C and D).

Previous studies showed that BCL2 has multiple phosphorylation sites (T69, S70, S87), and BCL2 phosphorylation inhibits its interaction with BECN1 to stimulate autophagosome formation. We wondered if poly-GR and poly-PR could promote BECN1−BCL2 interaction by reducing BCL2 phosphorylation. To test this possibility, we examined the level of endogenous BCL2 phosphorylation on S87 and S70 sites. Immunoblot experiments demonstrated that phosphorylation of BCL2 on both S87 and S70 sites decreased after poly-GR and poly-PR expression (Fig. 4E−G). To further confirm the mechanism underlying poly-GR and poly-PR-mediated inhibition of autophagosome formation, we knocked down the *BECN1* gene and checked the effect of poly-PR on autophagy. Our data showed that poly-PR failed to inhibit autophagy in starved cells lacking BECN1, suggesting that *C9orf72* arginine-rich DPRs regulate autophagosomal formation in a BECN1-dependent manner (Fig. 4H and I). Moreover, the similar results were obtained when we performed immunoblot analysis of LC3 (Fig. 4J and K). Taken together, our results demonstrated that *C9orf72* arginine-rich DPRs inhibit autophagosome formation by regulating BCL2 phosphorylation and BCL2−BECN1 interaction.

3.5. *SW063058 restores DPRs-inhibited autophagy through targeting BECN1−BCL2 interaction*

The process of autophagy is crucial to both cellular physiology and pathology. We wondered that whether restoring autophagy in DPR-expressing cells is benefit for cellular survival. According to the previous study, SW063058 is a small molecular compound which selectively disrupts the BECN1−BCL2 binding through BH3 domain of BECN1 to promote autophagy without inducing apoptosis[33]. Since we have found that DPRs dramatically impaired autophagy by increasing the BECN1−BCL2 binding, we sought to test effect of SW063058 on autophagy and toxicity in DPR-expressing cells. Our data showed that SW063058 treatment recovered autophagy in a dose-dependent manner in poly-PR-expressing cells under starvation (Fig. 5A−D), and the effective drug concentration was higher than 2 μmol/L. 10 μmol/L SW063058 strongly restored autophagy and disrupted BECN1−BCL2 binding in poly-PR-expressing cells (Fig. 5C−E).

To better understand the effect of DPRs on autophagy in neurons, we examined autophagy in primary cortical neurons expressing poly-PR. Importantly, upon on long-term EBSS treatment, poly-PR strikingly impaired autophagy and neurite outgrowth, which could be rescued by SW063058 treatment (Fig. 6A and B). Moreover, proximity ligation assay (PLA) was applied to assess the interactions between BECN1 and BCL2, and

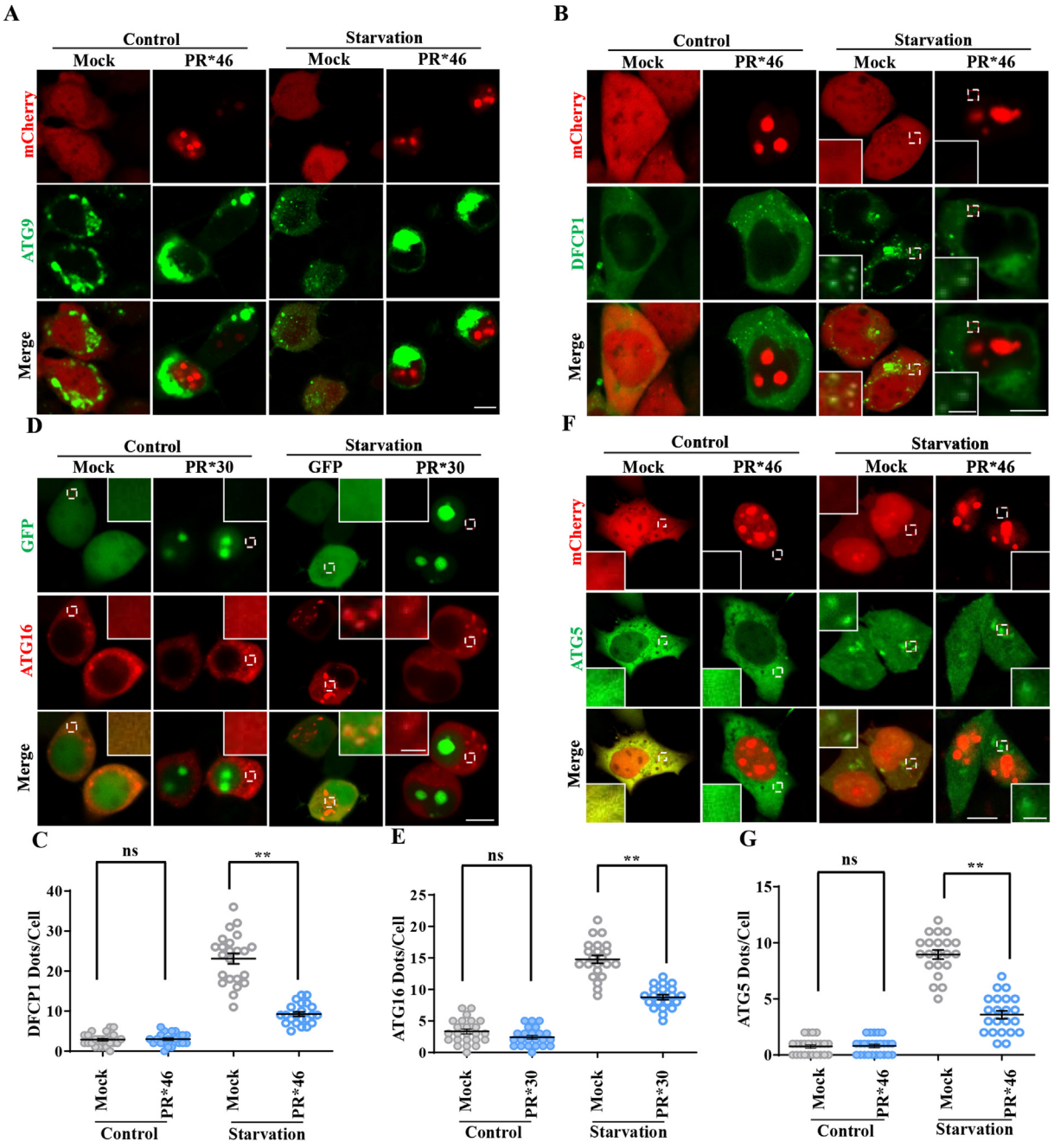

Figure 3 Poly-PR inhibits the initiation of autophagosomal biogenesis. (A) HEK 293 cells were transfected with ATG9-GFP and mCherry-PR*46 or mCherry tag (Mock). After 48 h, the cells were treated with EBSS for 1 h. Then, cells were visualized using confocal microscopy. Scale bar, 10 μm. (B) HEK 293 cells were transfected with DFCP1-GFP and mCherry-PR*46 or mCherry tag (Mock). After 48 h, the cells were starved for 1 h with EBSS. Then, cells were visualized using confocal microscopy. Scale bar, 10 μm. Insets were higher magnifications of the dashed box area. Scale bars, 2 μm. (C) The number of DFCP1 dots per cell in (B) was counted, and 20−30 cells in each group from three independent experiments were statistically analyzed. Data are represented as means ± SEM; ns, not significantly different; $^{**}P < 0.01$, one-way ANOVA. (D) HEK 293 cells were transfected with ATG16-mCherry and GFP-PR*30 or GFP tag (Mock). After 48 h, the cells were incubated with normal culture medium or EBSS for 1 h. Then, cells were visualized using confocal microscopy. Scale bar, 10 μm. Insets were higher magnifications of the dashed box area. Scale bars, 2 μm. (E) The number of ATG16 dots per cell was counted, and 20−30 cells in each group from three independent experiments were statistically analyzed. Data are represented as means ± SEM; ns, not significantly different; $^{**}P < 0.01$, one-way ANOVA. (F) HEK 293 cells were transfected with ATG5-GFP and mCherry-PR*46 or mCherry tag (Mock). After 48 h, the cells were incubated with normal culture medium or EBSS for 1 h Then, the cells were visualized using confocal microscopy. Scale bar, 10 μm. Insets were higher magnifications of the dashed box area. Scale bars, 2 μm. (G) The number of ATG5 dots per cell was counted, and 20−30 cells in each group from three independent experiments were statistically analyzed. Data are represented as means ± SEM; ns, not significantly different; $^{**}P < 0.01$, one-way ANOVA.

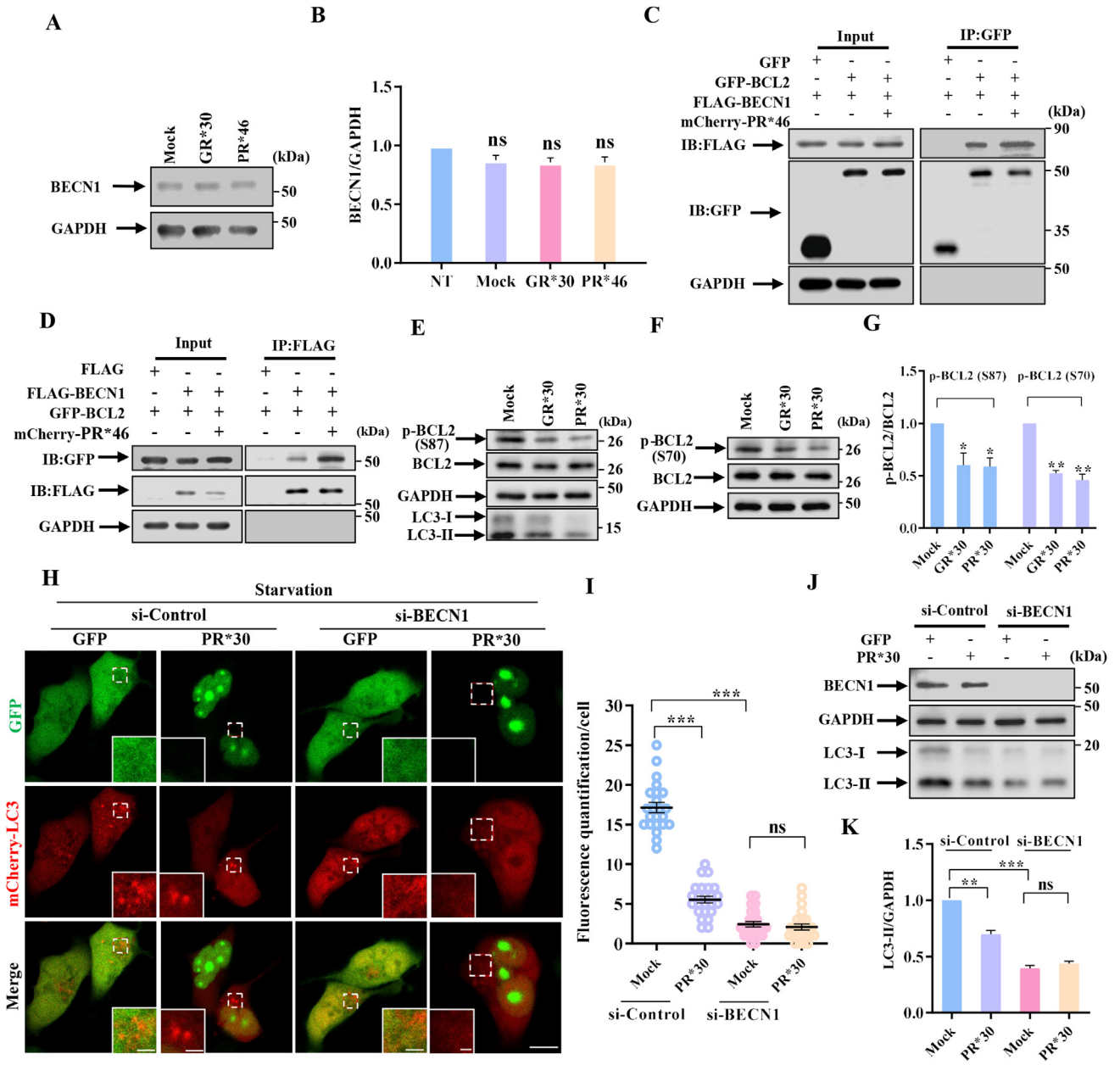

Figure 4 Poly-PR inhibits the autophagy by promoting the interaction between BECN1 and BCL2. (A, B) HEK 293 cells were transfected with GR*30, PR*46 or empty tag (Mock). After 48 h, cells lysates were subjected to immunoblot analysis using antibodies against BECN1 and GAPDH. The relative intensity of BECN1 to GAPDH are shown in (B). Data from three independent experiments are represented as means ± SEM; ns, not significantly different, one-way ANOVA. (C) HEK 293T cells were transfected with FLAG-BECN1 and GFP-BCL2 or GFP tag and mCherry-PR*46 or mCherry tag. After 48 h, the supernatants of the cell lysates were used in immunoprecipitation assay using GFP antibody. Bound proteins were detected with GFP, FLAG and GAPDH antibodies. (D) HEK 293T cells were transfected with GFP-BCL2 and FLAG-BECN1 or FLAG tag and mCherry-PR*46 or mCherry tag. After 48 h, the supernatants of the cell lysates were used in immunoprecipitation assay with FLAG antibody. Bound proteins were detected with GFP, FLAG and GAPDH antibodies. (E−G) HEK 293 cells were transfected with GFP-GR*30, GFP-PR*30 or GFP tag (Mock). After 48 h, cell lysates were subjected to immunoblot analysis using antibodies against phosphorylated BCL2 (S87) in (E) or phosphorylated BCL2 (S70) in (F), BCL2, LC3 and GAPDH. The relative intensity of phosphorylated BCL2 (S87) or (S70) to total BCL2 are shown in (G). Data from three independent experiments are represented as means ± SEM; $*P < 0.05$; $**P < 0.01$, one-way ANOVA. (H) HEK 293 cells were transfected with indicated siRNA for 48 h. Then the cells were re-transfected with mCherry-LC3 and GFP-PR*30 or GFP tag. After 24 h, the cells were incubated with EBSS for 1 h. Then, cells were visualized using confocal microscope. Scale bars, 10 μm. Insets were higher magnifications of the dashed box area. Scale bars, 2 μm. (I) The number of LC3 dots per cell in (H) was counted, and 20−30 cells in each group from three independent experiments were statistically analyzed. Data are represented as means ± SEM; ns, not significantly different; $***P < 0.001$, one-way ANOVA. (J, K) HEK 293 cells were similarly transfected and treated as in (H). Then, cells lysates were subjected to immunoblot analysis using antibodies against BECN1, LC3 and GAPDH. The relative intensity of LC3-II to GAPDH are shown in (K). Data from three independent experiments are represented as means ± SEM; ns, not significantly different; $**P < 0.01$; $***P < 0.001$, one-way ANOVA.

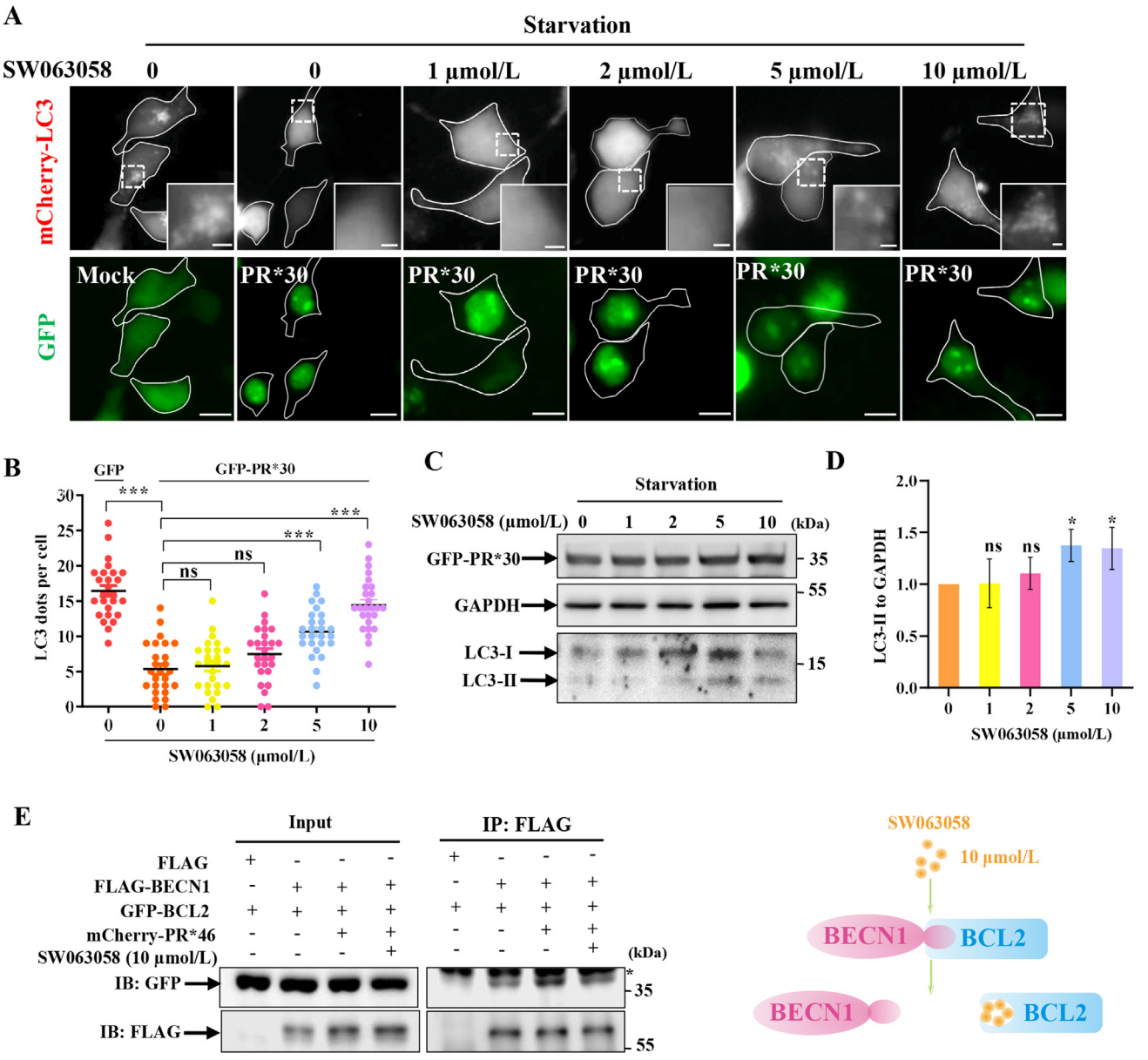

Figure 5 SW063058 alleviates *C9orf72* arginine-containing DPR-induced autophagy inhibition through specifically targeting to BCL2−BECN1 protein complex. (A) HEK 293 cells were transfected with mCherry-LC3 and GFP or GFP-PR*30, and then the cells were pre-treated with SW063058 at indicated concentrations for 11 h. The cells were incubated with EBSS for 1 h and visualized using fluorescence microscope. Scale bars, 10 μm. Insets were higher magnifications of the dashed box area. Scale bars, 2 μm. (B) The number of LC3 dots per cell in (A) was counted, and 20−30 cells in each group from three independent experiments were statistically analyzed. Data are represented as means ± SEM; ns, not significantly different; ***$P < 0.001$, one-way ANOVA. (C) HEK 293 cells were similarly transfected and treated as (A). The cell lysates were subjected to immunoblot with indicated antibodies. (D) The relative intensities in C from three independent experiments were presented as means ± SD; ns, not significantly different; *$P < 0.05$, one-way ANOVA. (E) HEK 293 cells were transfected with indicated plasmids and treated with 10 μmol/L SW063058 for 12 h. The supernatants of the cell lysates were used in immunoprecipitation assay using anti-FLAG antibody. * indicates IgG heave chains. Right region: schematic model illustrating the disruption of the interaction between BECN1 and BCL2 by SW063058.

poly-PR-expressing neurons displayed increased PLA signal, indicating the enhancement of BECN1−BCL2 binding (Fig. 6C and D). Whereas, the PLA signal was reduced by SW063058 treatment, suggesting the inhibition of BECN1−BCL2 interactions (Fig. 6C and D). Taken together, our data revealed that the impairment of autophagy may contribute to *C9orf72*-meidated neurotoxicity and provided a potential strategy (drug intervention of BECN1−BCL2 interaction) for *C9orf72*-linked ALS/FTD therapy (Fig. 6E).

4. Discussions

C9orf72-linked neurodegeneration is mainly recognized as gain-of-function disease, despite that loss of function mechanism may also contribute to disease pathogenesis due to transcriptional inhibition of *C9orf72* gene[3,4,6,19,20,34]. For the Protein/RNA gain of function mechanism, expanded hexanucleotide RNA and RAN translated DPR proteins, especially arginine-rich poly-GR and poly-PR, have both been shown to damage cells and contribute to *C9orf72*-linked

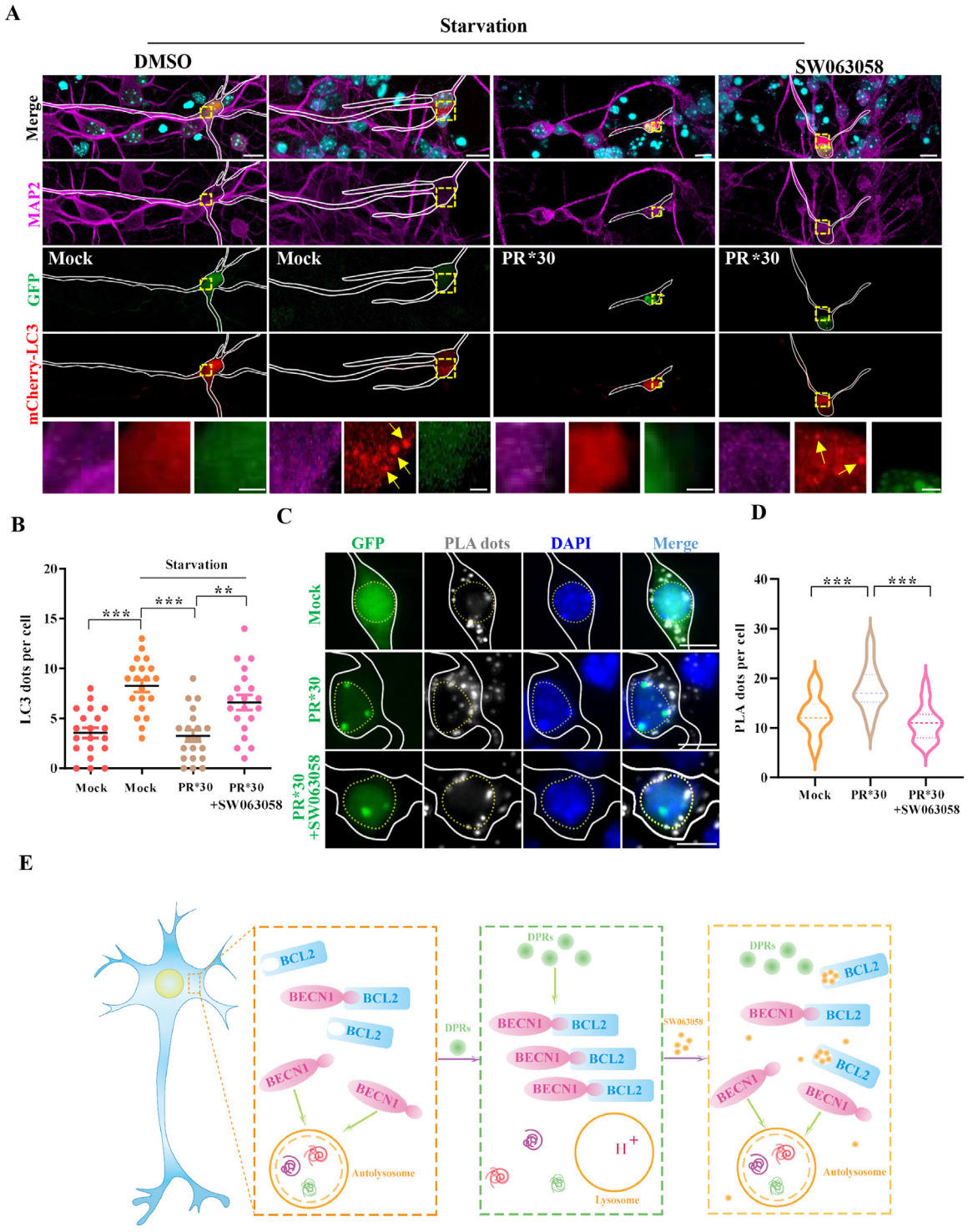

Figure 6 *C9orf72* arginine-containing DPRs impede neuronal autophagy. (A) Mouse cortical neurons (DIV 7) were transfected with mCherry-LC3 and GFP or GFP-PR*30, and then were pre-treated with SW063058 for 4 h. The neurons were incubated with EBSS for 8 h prior to immunofluorescent assay with anti-MAP2 antibody (magenta) and Hoechst (cyan). Scale bars, 10 μm. Insets were higher magnifications of the dashed box area. Scale bars, 2 μm. (B) The number of LC3 dots in soma per neuron in (A) was counted, and 20 neurons in each group from three independent experiments were statistically analyzed. Data are represented as mean ± SEM; $^{**}P < 0.01$; $^{***}P < 0.001$, one-way ANOVA. (C) Mouse cortical neurons (DIV 7) were transfected with GFP or GFP-PR*30. Images of in situ PLA using rabbit anti-BECN1 and mouse anti-BCL2 antibodies. Blue: nuclei (DAPI); white dots: PLA positive puncta. Scale bars, 10 μm. (D) The number of PLA dots per neuron in (C) was counted, and 20 somas of neuron in each group from three independent experiments were statistically analyzed. Data are represented as mean ± SEM; $^{***}P < 0.001$, one-way ANOVA. (E) The schematic model of this study. BECN1−BCL2 interaction regulates autophagy in cells. DPRs significantly inhibit neuronal autophagy by enhancing the interactions of BECN1 and BCL2. A small molecule compound SW063058 disrupts BECN1−BCL2 interaction, thereby restoring autophagy in DPR-expressing neurons.

ALS/FTD[1,6−11,35]. Interestingly, poly-GR and poly-PR are linked to impaired ribosomal biogenesis, an important step in protein quality control system. Here, we discuss how poly-GR and poly-PR may act to disrupt autophagy and contribute to *C9orf72*-linked ALS/FTD. Since defective autophagy is a common feature of neurodegenerative diseases that display abnormal protein aggregation in association with declined protein homeostasis[13,30], our findings link autophagy to the interaction between C9orf72-mediated pathogenesis and protein quality control system.

Although the role of *C9orf72* DPR-mediated autophagy dysfunction in ALS/FTD disease pathogenesis remains unclear, this pathway may participate in the disease progress in combination with other mechanisms including *C9orf72* loss of function. Interestingly, it has been shown that loss of *C9orf72* strongly link to autophagic regulation[19,34,36−40]. Therefore, the gain and loss of function mechanisms may coordinate together to facilitate the autophagic failure and disease progress. Also, given that altered *C9orf72* in both glial cells and neurons can complicate the disease pathogenesis, the potential contribution of *C9orf72*-mediated autophagy to ALS/FTD pathogenesis needs to be further explored in the future.

Induction of autophagy has therapeutic potential to treat neurodegenerative disorders, and there are several strategies to enhance the overall function of autophagy, including stimulation from the upstream signaling such as mTOC1 and/or TFEB which in turn increases the number of autophagosomes and lysosomes throughout the whole flux[18,30]. However, such strategies may not be helpful of the treatment of poly-GR and poly-PR-mediated neurotoxicity, since mTORC1 is already inhibited and TFEB stays in the active form (translocation into the nucleus) in cells expressing poly-GR and poly-PR (Supporting Information Fig. S3). In summary, the arginine-rich DPRs affects the interaction between BCL2 and BECN1 through modulating BCL2 phosphorylation (Figs. 4 and 5). This modulation in turn dominantly inhibits the ALP despite that mTOC1−TFEB signaling is activated, as indicated by the fluorescent reporter of autophagic degradation (Fig. 2E). Regarding the effect of DPRs on BCL2 phosphorylation, future study needs to check whether DPRs can direct interact with BCL2, or whether DPRs affect the upstream signaling that modulate BCL2 phosphorylation. Taken together, our data reveal a novel mechanism that poly-GR and poly-PR encoded by the *C9orf72* hexanucleotide repeat expansions may display "cytoplasmic toxicity" in combination with the previously reported nuclear toxicity[8,10,11].

It is worth to note that ALS can be considered as a "quality control disease" associated with dysfunction in RNA and protein homeostasis, since many proteins involved in RNA homeostasis (FUS, TDP-43, angiogenin, ataxin-2, hnRNPA1, hnRNPA2/B1, EWSR1, TAF15 and SETX) and ubiquitin−proteasome system (VCP and UBQLN2) or ALP (p62/SQSTM1, OPTN, TBK1 and VAPB) are genetically associated with ALS[2,16]. Thus, perturbed RNA and protein quality control was reasonably thought to be the critical mechanism underlying the pathogenesis of ALS/FTD. We and others previously identified that *C9orf72*-linked poly-GR and poly-PR could impair rRNA and ribosome biogenesis[8,11,41], which may therefore affect the global RNA and protein homeostasis. With this in mind, the current research highlights autophagy as an important protein quality control system in poly-GR and poly-PR-mediated neurodegeneration, suggesting that RNA and protein quality control systems may coordinately contribute to ALS/FTD pathogenesis.

5. Conclusions

The present study identifies BCL2−BECN1 protein complex, which functions as the key component in the regulation of autophagy, is a novel drug target of *C9orf72*-linked ALS/FTD. We show that *C9orf72* arginine-enriched DPRs, including poly-GR and poly-PR, can increase the interaction between BCL2 and BECN1 through reducing BCL2 phosphorylation, therefore the arginine-containing DPRs can impair the overall function of autophagy and the clearance of protein aggregates in association with neurodegenerative diseases. Importantly, we show that pharmacological inhibition of BCL2−BECN1 interaction, using small molecule compound SW063058, displays protective effect in neuron model of *C9orf72*-linked ALS/FTD.

Acknowledgements

We thank Dr. Guanghui Wang, Dr. Zhouteng Tao, Dr. Zongbing Hao and Dan Wu for the experimental materials and stimulating discussions. Due to space limitation, we did not include all the references, therefore we apologize to the researches whose references are missing in this paper. This work was supported by the National Natural Science Foundation of China (Nos. 82022022, 32371018 and 82071274), a Project Funded by Jiangsu Key Laboratory of Neuropsychiatric Diseases (BM2013003, China), a Key Project of Natural Science Foundation of Jiangsu Provincial Higher Education Institutions (23KJA310005, China), a Project Funded by the Interdisciplinary Basic Frontier Innovation Program of Suzhou Medical College of Soochow University (MP13202823, China), a Project Funded by the Suzhou International Joint Laboratory for Diagnosis and Treatment of Brain Diseases, and a Project Funded by the Priority Academic Program Development of the Jiangsu Higher Education Institutes (PAPD). J.H.M.P. was supported Science Foundation Ireland (17/COEN/3474, 17/JPND/3455). Q.M. is a recipient of an RCSI International StAR Ph.D. scholarship. N.L. was supported by the Postgraduate Research & Practice Innovation Program of Jiangsu Province. K.Y.T., was supported by the financial support from the Science and Technology Development Fund, Macau SAR (File no. 0062/2021/A, China) and University of Macau (File no. MYRG2022-00171-FHS, China).

Author contributions

Zheng Ying, Hongfeng Wang, Shiqiang Xu and Qilian Ma designed research; Shiqiang Xu, Qilian Ma, Junwen Shen, Ningning Li, Shan Sun, Nana Wang. Yang Chen and Chunsheng Dong performed experiments; Shiqiang Xu, Qilian Ma, Kin Yip Tam, Jochen H. M. Prehn, Hongfeng Wang and Zheng Ying analyzed data; Shiqiang Xu, Qilian Ma, Hongfeng Wang and Zheng Ying wrote the paper.

Conflicts of interest

The authors have no conflict to declare.

Appendix A. Supporting information

Supporting data to this article can be found online at https://doi.org/10.1016/j.apsb.2024.02.004.

References

1. Donnelly CJ, Zhang PW, Pham JT, Heusler AR, Mistry NA, Vidensky S, et al. RNA toxicity from the ALS/FTD C9ORF72 expansion is mitigated by antisense intervention. *Neuron* 2013;**80**:415−28.
2. Taylor JP, Brown Jr RH, Cleveland DW. Decoding ALS: from genes to mechanism. *Nature* 2016;**539**:197−206.
3. DeJesus-Hernandez M, Mackenzie IR, Boeve BF, Boxer AL, Baker M, Rutherford NJ, et al. Expanded GGGGCC hexanucleotide repeat in noncoding region of C9ORF72 causes chromosome 9p-linked FTD and ALS. *Neuron* 2011;**72**:245−56.
4. Renton AE, Majounie E, Waite A, Simon-Sanchez J, Rollinson S, Gibbs JR, et al. A hexanucleotide repeat expansion in C9ORF72 is the cause of chromosome 9p21-linked ALS-FTD. *Neuron* 2011;**72**:257−68.
5. Gijselinck I, Van Langenhove T, van der Zee J, Sleegers K, Philtjens S, Kleinberger G, et al. A C9orf72 promoter repeat expansion in a Flanders-Belgian cohort with disorders of the frontotemporal lobar degeneration-amyotrophic lateral sclerosis spectrum: a gene identification study. *Lancet Neurol* 2012;**11**:54−65.
6. Balendra R, Isaacs AM. C9orf72-mediated ALS and FTD: multiple pathways to disease. *Nat Rev Neurol* 2018;**14**:544−58.
7. Swinnen B, Robberecht W, Van Den Bosch L. RNA toxicity in non-coding repeat expansion disorders. *EMBO J* 2020;**39**:e101112.
8. Kwon I, Xiang S, Kato M, Wu L, Theodoropoulos P, Wang T, et al. Poly-dipeptides encoded by the C9orf72 repeats bind nucleoli, impede RNA biogenesis, and kill cells. *Science* 2014;**345**:1139−45.
9. Mizielinska S, Gronke S, Niccoli T, Ridler CE, Clayton EL, Devoy A, et al. C9orf72 repeat expansions cause neurodegeneration in *Drosophila* through arginine-rich proteins. *Science* 2014;**345**:1192−4.
10. Wen X, Tan W, Westergard T, Krishnamurthy K, Markandaiah SS, Shi Y, et al. Antisense proline-arginine RAN dipeptides linked to C9ORF72-ALS/FTD form toxic nuclear aggregates that initiate *in vitro* and *in vivo* neuronal death. *Neuron* 2014;**84**:1213−25.
11. Tao Z, Wang H, Xia Q, Li K, Jiang X, Xu G, et al. Nucleolar stress and impaired stress granule formation contribute to C9orf72 RAN translation-induced cytotoxicity. *Hum Mol Genet* 2015;**24**:2426−41.
12. Wong E, Cuervo AM. Autophagy gone awry in neurodegenerative diseases. *Nat Neurosci* 2010;**13**:805−11.
13. Nguyen DKH, Thombre R, Wang J. Autophagy as a common pathway in amyotrophic lateral sclerosis. *Neurosci Lett* 2019;**697**:34−48.
14. Hara T, Nakamura K, Matsui M, Yamamoto A, Nakahara Y, Suzuki-Migishima R, et al. Suppression of basal autophagy in neural cells causes neurodegenerative disease in mice. *Nature* 2006;**441**:885−9.
15. Komatsu M, Waguri S, Chiba T, Murata S, Iwata J, Tanida I, et al. Loss of autophagy in the central nervous system causes neurodegeneration in mice. *Nature* 2006;**441**:880−4.
16. Ling SC, Polymenidou M, Cleveland DW. Converging mechanisms in ALS and FTD: disrupted RNA and protein homeostasis. *Neuron* 2013;**79**:416−38.
17. Xia Q, Wang H, Hao Z, Fu C, Hu Q, Gao F, et al. TDP-43 loss of function increases TFEB activity and blocks autophagosome−lysosome fusion. *EMBO J* 2016;**35**:121−42.
18. Puertollano R, Ferguson SM, Brugarolas J, Ballabio A. The complex relationship between TFEB transcription factor phosphorylation and subcellular localization. *EMBO J* 2018;**37**:e98804.
19. Ugolino J, Ji YJ, Conchina K, Chu J, Nirujogi RS, Pandey A, et al. Loss of C9orf72 enhances autophagic activity *via* deregulated mTOR and TFEB signaling. *PLoS Genet* 2016;**12**:e1006443.
20. Wang M, Wang H, Tao Z, Xia Q, Hao Z, Prehn JHM, et al. C9orf72 associates with inactive Rag GTPases and regulates mTORC1-mediated autophagosomal and lysosomal biogenesis. *Aging Cell* 2020;**19**:e13126.
21. Zhang ZL, Wang HF, Ding QF, Xing YF, Xu DL, Xu ZH, et al. The tumor suppressor p53 regulates autophagosomal and lysosomal biogenesis in lung cancer cells by targeting transcription factor EB. *Biomed Pharmacother* 2017;**89**:1055−60.
22. Zhang ZL, Wang NN, Ma QL, Chen Y, Yao L, Zhang L, et al. Somatic and germline mutations in the tumor suppressor gene impair PINK1/Parkin-mediated mitophagy in lung cancer cells. *Acta Pharmacol Sin* 2020;**41**:93−100.
23. Chen Y, Xu SQ, Wang NN, Ma QL, Peng PP, Yu YH, et al. Dynasore suppresses mTORC1 activity and induces autophagy to regulate the clearance of protein aggregates in neurodegenerative diseases. *Neurotox Res* 2019;**36**:108−16.
24. Zhou L, Wang HF, Ren HG, Chen D, Gao F, Hu QS, et al. Bcl-2-dependent upregulation of autophagy by sequestosome 1/p62 *in vitro*. *Acta Pharmacol Sin* 2013;**34**:651−6.
25. Xia Q, Hu Q, Wang H, Yang H, Gao F, Ren H, et al. Induction of COX-2−PGE2 synthesis by activation of the MAPK/ERK pathway contributes to neuronal death triggered by TDP-43-depleted microglia. *Cell Death Dis* 2015;**6**:e1702.
26. Fang LM, Li B, Guan JJ, Xu HD, Shen GH, Gao QG, et al. Transcription factor EB is involved in autophagy-mediated chemoresistance to doxorubicin in human cancer cells. *Acta Pharmacol Sin* 2017;**38**:1305−16.
27. Guo DK, Zhu Y, Sun HY, Xu XY, Zhang S, Hao ZB, et al. Pharmacological activation of REV-ERBα represses LPS-induced microglial activation through the NF-κB pathway. *Acta Pharmacol Sin* 2019;**40**:26−34.
28. Wang H, Wang N, Xu D, Ma Q, Chen Y, Xu S, et al. Oxidation of multiple MiT/TFE transcription factors links oxidative stress to transcriptional control of autophagy and lysosome biogenesis. *Autophagy* 2019;**16**:1683−96.
29. Kaizuka T, Morishita H, Hama Y, Tsukamoto S, Matsui T, Toyota Y, et al. An autophagic flux probe that releases an internal control. *Mol Cell* 2016;**64**:835−49.
30. Dikic I, Elazar Z. Mechanism and medical implications of mammalian autophagy. *Nat Rev Mol Cell Biol* 2018;**19**:349−64.
31. Pattingre S, Tassa A, Qu X, Garuti R, Liang XH, Mizushima N, et al. Bcl-2 antiapoptotic proteins inhibit Beclin 1-dependent autophagy. *Cell* 2005;**122**:927−39.
32. Wei Y, Pattingre S, Sinha S, Bassik M, Levine B. JNK1-mediated phosphorylation of Bcl-2 regulates starvation-induced autophagy. *Mol Cell* 2008;**30**:678−88.
33. Chiang WC, Wei Y, Kuo YC, Wei S, Zhou A, Zou Z, et al. High-throughput screens to identify autophagy inducers that function by disrupting Beclin 1/Bcl-2 binding. *ACS Chem Biol* 2018;**13**:2247−60.
34. Boivin M, Pfister V, Gaucherot A, Ruffenach F, Negroni L, Sellier C, et al. Reduced autophagy upon C9ORF72 loss synergizes with dipeptide repeat protein toxicity in G4C2 repeat expansion disorders. *EMBO J* 2020;**39**:e100574.
35. Haeusler AR, Donnelly CJ, Periz G, Simko EA, Shaw PG, Kim MS, et al. C9orf72 nucleotide repeat structures initiate molecular cascades of disease. *Nature* 2014;**507**:195−200.
36. Sullivan PM, Zhou X, Robins AM, Paushter DH, Kim D, Smolka MB, et al. The ALS/FTLD associated protein C9orf72 associates with SMCR8 and WDR41 to regulate the autophagy−lysosome pathway. *Acta Neuropathol Commun* 2016;**4**:51.
37. Yang M, Liang C, Swaminathan K, Herrlinger S, Lai F, Shiekhattar R, et al. A C9ORF72/SMCR8-containing complex regulates ULK1 and plays a dual role in autophagy. *Sci Adv* 2016;**2**:e1601167.
38. Webster CP, Smith EF, Bauer CS, Moller A, Hautbergue GM, Ferraiuolo L, et al. The C9orf72 protein interacts with Rab1a and the ULK1 complex to regulate initiation of autophagy. *EMBO J* 2016;**35**:1656−76.
39. Sellier C, Campanari ML, Julie Corbier C, Gaucherot A, Kolb-Cheynel I, Oulad-Abdelghani M, et al. Loss of C9ORF72 impairs autophagy and synergizes with polyQ Ataxin-2 to induce motor neuron dysfunction and cell death. *EMBO J* 2016;**35**:1276−97.
40. Ho WY, Tai YK, Chang JC, Liang J, Tyan SH, Chen S, et al. The ALS-FTD-linked gene product, C9orf72, regulates neuronal morphogenesis *via* autophagy. *Autophagy* 2019;**15**:827−42.
41. Hartmann H, Hornburg D, Czuppa M, Bader J, Michaelsen M, Farny D, et al. Proteomics and C9orf72 neuropathology identify ribosomes as poly-GR/PR interactors driving toxicity. *Life Sci Alliance* 2018;**1**:e201800070.